Sound & Vibration 2025, 59(1), 2048.
https://doi.org/10.59400/sv2048

Article

Design optimization of vibration amplitude reduction based on virtual prototype and machine learning

Hong Bao[1,2], Jinxuan Tao[1,2], Jing Yang[1,2], Bin Cao[3], Liuxian Zhao[2,*]

[1] Anhui Province Key Laboratory of Low Carbon Recycling Technology and Equipment for Mechanical and Electrical Products, Hefei University of Technology, Hefei 230000, China
[2] School of mechanical engineering, Hefei University of Technology, Hefei 230000, China
[3] Industrial Training Centre, Hefei University of Technology, Hefei 230000, China
*** Corresponding author:** Liuxian Zhao, lxzhao@hfut.edu.cn

CITATION

Bao H, Tao J, Yang J, et al. Design optimization of vibration amplitude reduction based on virtual prototype and machine learning. Sound & Vibration. 2025; 59(1): 2048. https://doi.org/10.59400/sv2048

ARTICLE INFO

Received: 25 April 2024
Accepted: 14 November 2024
Available online: 19 December 2024

Abstract: The traditional design optimization of vibration amplitude reduction mainly has the disadvantages of low modeling and prediction accuracy as well as low optimization efficiency. Therefore, this paper presents a design optimization method for vibration amplitude reduction based on virtual prototyping and machine learning, which combines the high accuracy of numerical calculations with the efficiency of machine learning, overcoming the shortcomings of traditional methods. Firstly, sample points are collected through the design of experiments and virtual prototype simulation. Then, based on the sampled data, a prediction model for the relationship between the design parameters and the amplitude of the product is established using Genetic Algorithm-Support Vector Regression (GA-SVR). On the basis of the GA-SVR prediction model, a multi-objective optimization model of product is established, and Multiple Objectives Particle Swarm Optimization -entropy weight- Technique for Order Preference by Similarity to Ideal Solution (MOPSO-entropy weight-TOPSIS) is used to solve for the optimal design parameters. Finally, the washing machine suspension system is used as an example to verify the effectiveness of the model. The results show that, compared with the original design scheme, the design scheme obtained by the model can reduce the amplitude of the washing machine suspension system by 12.68%, and reduce the total weight of the counterweight by 7.35%. This method is conducive to the intelligent and efficient design optimization of vibration amplitude reduction, and is of great significance to product life cycle design.

Keywords: vibration amplitude reduction optimization design; virtual prototype; machine learning; MOPSO-entropy weight-TOPSIS; washing machine suspension system

1. Introduction

The harmful vibration amplitude of a product can seriously affect its performance. For products with specific vibration performance requirements, design optimization to reduce vibration amplitude is indispensable for life cycle design. Current research proposes two design optimization methods for vibration amplitude reduction, mainly focusing on different phases. The first method involves proceeding from the theoretical model of multi-body dynamics, predicting and analyzing the dynamic characteristics of the product by establishing the dynamic model of the multi-body system within the product, and further achieving design optimization. Wang et al. [1] established the vibration differential equation of the suspension system of a drum washing machine by using the Lagrange equation, which reflects the actual vibration characteristics of the washing machine. Kim et al. [2] analyzed the vibration characteristics of a wave washing machine with a four-way horizontal vibration

damping system through a dynamic model and Newtonian mechanics. Mendoza-Flores et al. [3] studied the dynamic characteristics of displacement, velocity, and acceleration of the center of mass of a horizontal washing machine by establishing a dynamic model. Tong et al. [4] established a dynamic model of the Particle Damping Vibration Absorber-Jib-Cargo Coupling System (PDVA-J-C-CS) based on Euler-Bernoulli beam theory and the Lagrange equation to address the issues of large vibrations of the jib and cargo swing in flat-top tower cranes. The dynamic characteristics are effectively predicted by establishing a theoretical model of multi-body dynamics.

However, the prediction results of the dynamic characteristics are not accurate due to the inevitable simplification of the theoretical model. The second method uses numerical calculation methods based on virtual prototype simulation to predict dynamic characteristics. Cha et al. [5] established a virtual prototype model of the washing machine suspension system based on ADAMS/View to predict amplitude. Xiao et al. [6] established a rigid-flexible coupling model of the suspension system of a drum washing machine in ADAMS/Vibration based on the Lagrange method, which improved the accuracy of the calculation of the vibration response of the suspension system. Le et al. [7] and Totu et al. [8] studied the dynamic characteristics of a vehicle suspension system by establishing a numerical simulation model based on a virtual prototype. Wang et al. [9] built a virtual prototype of the vehicle suspension system on the ADAMS software platform to verify the vibration damping performance of the whole vehicle active suspension system under the backward-step fast terminal sliding mode control method based on the extended state observer. Guan et al. [10] analyzed the influence of parameter changes on vibration reduction and energy collection performance by establishing a virtual prototype model of a bionic suspension. The numerical calculation method has the advantage of solving complex problems accurately, which effectively improves the prediction accuracy of dynamic characteristics and is conducive to the realization of design optimization of vibration amplitude reduction.

However, numerical calculation is time-consuming when solving complex problems, which leads to disadvantages such as long design time and low efficiency in the design optimization of vibration amplitude reduction based on a virtual prototype. The data-driven method provides an opportunity to overcome these disadvantages. Machine learning algorithms can quickly establish surrogate models for numerical calculations with good accuracy using a small amount of sample data. The research method that combines numerical calculation with machine learning algorithms has been widely used in various fields and has achieved good results. Kashfi et al. [11] studied the plastic properties of a thick aluminum plate by combining finite element numerical simulation with Gaussian regression. Yu et al. [12] optimized fixture design based on finite element analysis and machine learning algorithms. Noh et al. [13] applied numerical calculation and support vector regression to optimize the indoor bicycle handle frame. Huri et al. [14] optimized the automotive rubber bumper using the finite element method and support vector regression. Liu et al. [15] applied finite element technology and support vector regression to design a polymeric thermal actuator.

Based on the above analysis, this article introduces a pioneering approach to vibration reduction and amplitude optimization by integrating virtual prototyping with machine learning techniques. Unlike traditional methods that primarily rely on numerical simulations, our approach leverages both high-fidelity simulation models and data-driven machine learning algorithms. A key innovation is the introduction of a vibration amplitude prediction model based on Support Vector Regression (SVR), which proves to be robust and effective, particularly in scenarios with limited data, demonstrating superior performance compared to other machine learning algorithms. By combining virtual prototyping and SVR-based predictions, our method enhances design efficiency, accelerates the optimization process, and provides engineers with proactive solutions. This approach enables the early detection of vibration issues in applications such as automotive and washing machine suspension systems. By combining virtual prototyping with SVR-based prediction, engineers can optimize designs to reduce vibrations, enhance stability, and extend component lifespan, making the design process more efficient. This paper is organized as follows: Section 2 introduces the methodology used in this paper. Section 3 uses the suspension system of a washing machine as an example to validate the effectiveness of the design optimization method for vibration amplitude reduction. Section 4 concludes this paper and presents future research.

2. Methodology

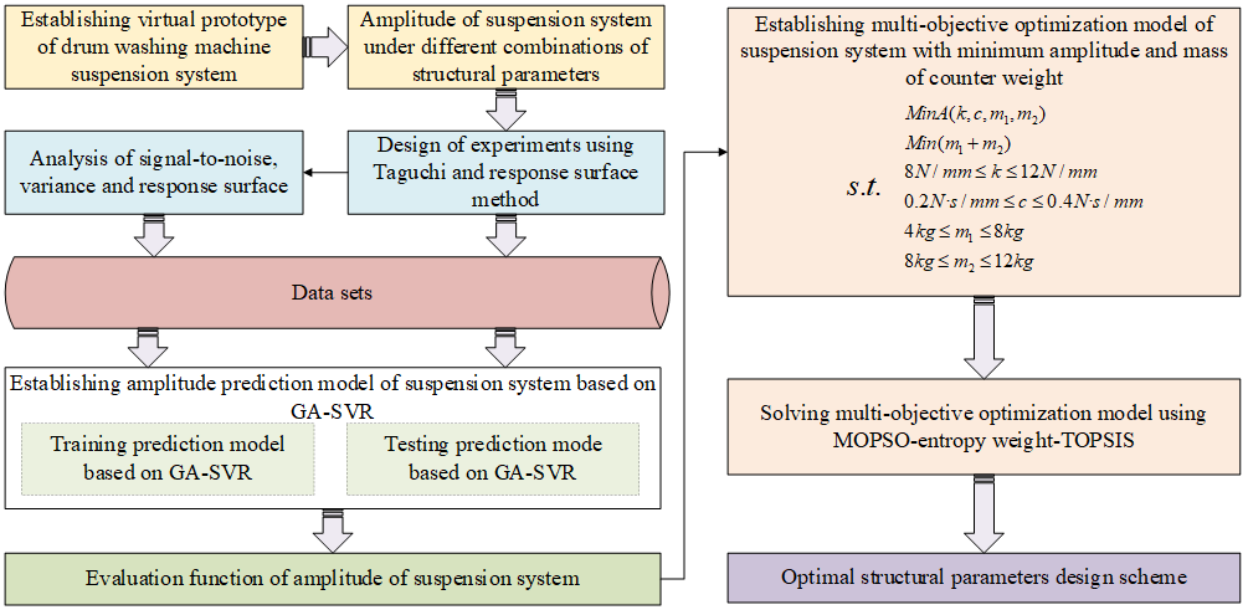

Figure 1. Design optimization method of vibration amplitude reduction based on virtual prototype and machine learning.

The specific implementation process of the design optimization method for reducing vibration amplitude, based on virtual prototype and machine learning, proposed in this paper is shown in **Figure 1**. First of all, the design of experiment is conducted to collect sample data, and the response results are obtained by numerical calculation based on virtual prototype simulations. Secondly, the vibration amplitude prediction model is established based on support vector regression using the collected

sample data. Then, the vibration amplitude optimization model is formulated using the predicted results from the model. Finally, the MOPSO-entropy weight-TOPSIS method is used to solve the optimization model and obtain the optimal design scheme.

2.1. Support vector regression

SVR is one of the machine learning algorithms widely used in modeling and prediction. As a machine learning algorithm with supervised learning, SVR has the advantage of processing a small sample size and high-dimensional nonlinear data sets.

For the input structural parameters x and output suspension system amplitude $f(\mathrm{x})$, the support vector regression model in the following form [16]:

$$f(\mathrm{x}) = \omega^T \varphi(\mathrm{x}) + b \tag{1}$$

where x is input vector, $\varphi(\mathrm{x})$ is the mapped eigenvector,ω and b are parameters of model. According to the principle of minimizing structural risk, ω and b can be obtained through solving the following constrained optimization problem:

$$\begin{aligned} &\min_{\omega,b,\xi_i,\zeta_i} \frac{1}{2}\|\omega\|^2 + C\sum_{i=1}^{m}\left(\xi_i + \hat{\xi}_i\right) \\ s.t.\ &f(\mathbf{x_i}) - y_i \le \varepsilon + \xi_i \\ &y_i - f(\mathbf{x_i}) \le \varepsilon + \hat{\xi}_i, \\ &\xi_i \ge 0, \zeta_i \ge 0, i = 1,2,\ldots,m. \end{aligned} \tag{2}$$

where C represents the regularization term, ξ_i and $\hat{\xi}_i$ represent relaxation variables, ε is the deviation between the predicted value and the actual value, m is the number of training set samples.

Introducing Lagrange multiplier $\mu_i > 0, \hat{\mu}_i > 0, \alpha_i > 0, \hat{\alpha}_i > 0$ to solve the above constrained optimization problem. The following Lagrange function is obtained by Lagrange multiplier method:

$$\begin{aligned} &L\left(\omega, b, \alpha, \hat{\alpha}, \xi, \hat{\xi}, \mu, \hat{\mu}\right) \\ &= \frac{1}{2}\|\omega\|^2 + C\sum_{i=1}^{m}\left(\xi_i + \hat{\xi}_i\right) - \sum_{i=1}^{m}\mu_i\xi_i - \sum_{i=1}^{m}\hat{\mu}_i\hat{\xi}_i + \sum_{i=1}^{m}\alpha_i(f(x_i) - y_i - \varepsilon - \xi_i) \\ &+ \sum_{i=1}^{m}\hat{\alpha}_i(y_i - f(x_i) - \varepsilon - \hat{\xi}_i) \end{aligned} \tag{3}$$

Substituting Equation (1) into (3), making partial derivative of $L(\omega, b, \alpha, \hat{\alpha}, \xi, \hat{\xi}, \mu, \hat{\mu})$ over ω equals zero, then the following equation can be obtained:

$$\omega = \sum_{i=1}^{m}(\hat{\alpha}_i - \alpha_i)\,\varphi(x_i) \tag{4}$$

The following support vector regression model can be obtained via substituting (4) into (1):

$$f(x) = \sum_{i=1}^{m}(\hat{\alpha}_i - \alpha_i)\kappa(x, x_i) + b \tag{5}$$

where $\kappa(x_i, x_j) = \varphi(x_i)^T \varphi(x_j)$ is a kernel function, the following Gaussian kernel function is selected in this paper:

$$\kappa(x_i, x_j) = exp(-\frac{\|x_i - x_j\|^2}{2\sigma^2}) \tag{6}$$

The prediction performance of SVR depends on the type of support vector machine, the kernel function and parameters of the model. In this paper, the type of support vector machine is $\varepsilon - SVR$, the kernel function is the Gaussian kernel function, and the parameters of the model are obtained by the genetic algorithm. The modelling and predicting of GA-SVR are achieved using LIBSVM [17].

2.2. Multiple objectives particle swarm optimization algorithm

The Multiple Objectives Particle Swarm Optimization (MOPSO) algorithm [18] is an extension of Particle Swarm Optimization (PSO), which has the advantage of a simple algorithm and rapid computation compared to other multi-objective algorithms, making it an effective method for multi-objective optimization problems. The main calculation steps are as follows:

Step 1: Initializing algorithm parameters such as population size, iteration numbers, social coefficient, cognitive coefficient, inertia weight, etc.

Step 2: Calculating the target vector corresponding to each particle in the population based on the fitness function value.

Step 3: Filtering non-dominated solutions in the particle swarm and updating the archive set. According to the dominance relationship, non-dominant solutions in the particle swarm are screened, inferior solutions are removed, and Pareto optimal solutions are added to the archive set. When the number of particles exceeds the capacity of the archive set, redundant particles are cleared based on the congestion distance.

Step 4: Update the velocity and position of each particle using the iteration equation of the velocity and position. The velocity and the position of the particles can be updated by the following equations:

$$v_{id}(t+1) = \omega v_{id}(t) + c_1 r_1 (p_{id}(t) - x_{id}(t)) + c_2 r_2 (g_d(t) - x_{id}(t)) \tag{7}$$

$$x_{id}(t+1) = x_{id}(t) + v_{id}(t+1) \tag{8}$$

where c_1, c_2 are the social coefficient and cognitive coefficient, t is the iteration number, r_1, $r_2$are random values from 0 to 1, ω is the inertia weight, which is used to control particle velocities.

Step 5: When the criteria of population stagnation under multi-objective optimization are met or the maximum number of iteration is reached, the algorithm is terminated and the external archive set is obtained.

2.3. Entropy weight-TOPSIS

The Technique for Order Preference by Similarity to Ideal Solution (TOPSIS) method makes decisions based on multi-objective evaluation of the alternatives through the standardized processing of the original data, which has the advantages of authenticity, intuition and reliability. However, the weight coefficient determined by

the TOPSIS method is subjective. The entropy weight-TOPSIS method [19] determines the weight coefficient objectively by introducing the entropy weight method.

The steps of this algorithm are summarized as follows [20]:

(1) Defining the alternative schemes and index attributes using decision matrix:

$$X = \begin{bmatrix} x_{11} & x_{12} & \cdots & x_{1n} \\ x_{21} & x_{22} & \cdots & x_{2n} \\ \vdots & \vdots & \vdots & \vdots \\ x_{m1} & x_{m2} & \cdots & x_{mn} \end{bmatrix} \tag{9}$$

where m is the number of alternative schemes, and n is the number of index attributes.

(2) Normalizing the decision matrix:

$$z_{ij} = \frac{x_{ij}}{\sqrt{\sum_{i=1}^{m} x_{ij}^2}}, i = 1, \ldots, m; j = 1, \ldots, n \tag{10}$$

(3) Determination of the index weight coefficient based on entropy weight method. The weight coefficient ω_j of index attributes were calculated via calculating the entropy e_j and difference coefficient g_j:

$$e_j = -\frac{1}{ln\, m} \sum_{i=1}^{m} \left(\frac{z_{ij}}{\sum_{i=1}^{m} z_{ij}} ln \frac{z_{ij}}{\sum_{i=1}^{m} z_{ij}} \right), i = 1, \ldots, m; j = 1, \ldots, n \tag{11}$$

$$g_j = 1 - e_j, i = 1, \ldots, m; j = 1, \ldots, n \tag{12}$$

$$\omega_j = \frac{g_j}{\sum_{j=1}^{n} g_j}, i = 1, \ldots, m; j = 1, \ldots, n \tag{13}$$

(4) Normalizing the matrix weighting. The normalized results of the decision matrix that considered the weighting coefficient of index attributes as following:

$$Z_{ij} = \omega_j z_{ij} \tag{14}$$

(5) Calculating the ideal solution and negative ideal solution of decision matrix Z_J^+, Z_J^-, and the Euclidean distance from the alternative schemes to the ideal solution and negative ideal solution S_i^+, S_i^-.

$$Z_J^+ = \{(\underset{i}{max} Z_{ij} | j \in J), (\underset{i}{min} Z_{ij} | j \in J')\} \tag{15}$$

$$Z_J^- = \{(\underset{i}{min} Z_{ij} | j \in J), (\underset{i}{max} Z_{ij} | j \in J')\} \tag{16}$$

$$S_i^+ = \sqrt{\sum_{j=1}^{n} (Z_{ij} - Z_j^+)^2}, \quad i = 1, \ldots, m \tag{17}$$

$$S_i^- = \sqrt{\sum_{j=1}^{n} (Z_{ij} - Z_j^-)^2}, \quad i = 1, \ldots, m \tag{18}$$

(6) Ranking of the alternative schemes. Calculating the relative closeness between each alternative schemes and the ideal solution, so as to rank the alternative schemes.

$$C_i^+ = \frac{S_i^-}{(S_i^+ + S_i^-)}, \quad i = 1, \ldots, m \tag{19}$$

The larger value of C_i^+, the closer the alternative schemes to the ideal solution, and the higher the ranking is.

3. Case study

This paper uses the washing machine suspension system as an example to verify the effectiveness of the proposed design optimization method for reducing vibration amplitudes. The suspension system, an essential component of the washing machine, comprises the inner cylinder, outer cylinder, dampers, springs, upper counterweight, lower counterweight, box baseplate, and motor. Excessive vibration amplitudes in the suspension system can pose the risk of the washing machine's box being impacted.

3.1. Design of experiment

Design of experiments based on the Taguchi method and the response surface method was conducted to collect the sample data in this paper. The structural parameters and factor levels considered in the experiment are shown in **Table 1**. These structural parameters and factor levels were determined by engineers based on existing design experience and the actual working conditions of the equipment. A total of 27 groups of sample data were obtained using the Taguchi method, and 30 groups of sample data were obtained using the response surface method-based design of experiments.

Table 1. Structural parameters and factor levels.

Factor levels	Stiffness coefficient of spring(N/mm)	Damping coefficient of damper(N·s/mm)	Mass of upper counter weight(kg)	Mass of lower counter weight(kg)
1	8	0.2	4	8
2	10	0.3	6	12
3	12	0.4	8	16

3.2. Simulation calculation of suspension system based on virtual prototype

3.2.1. Establishing virtual prototype simulation model of suspension system

The following assumptions were made in the virtual prototype numerical model: 1) The friction between the moving pairs is ignored, except for the friction damping in the damper; 2) The spring and damper are flexibly connected, and other parts are regarded as rigid bodies; 3) Both the spring and damper are linear models; 4) The eccentric mass, which represents the weight of the laundry, is fixed to the inner cylinder; 5) The baseplate of the box is fixed to the ground.

In this paper, the virtual prototype simulation of the suspension system was conducted using ADAMS. Based on the aforementioned assumptions and considering the actual connections, the constraints between components in the model were defined and presented in **Table 2**. The simulation model of the suspension system based on the virtual prototype has been established, as shown in **Figure 2**.

Table 2. Constraints among the components in the numerical model.

Component 1	Component 2	Joint
Inner cylinder	Outer cylinder	Revolute
Outer cylinder	Upper counter weight	Fixed
Outer cylinder	Lower counter weight	Fixed
Outer cylinder	Upper part of damper	Spherical
Box baseplate	Lower part of damper	Cylindrical
Upper part of damper	Lower part of damper	Translation
Box baseplate	Ground	Fixed
Inner cylinder	Eccentric mass	Fixed

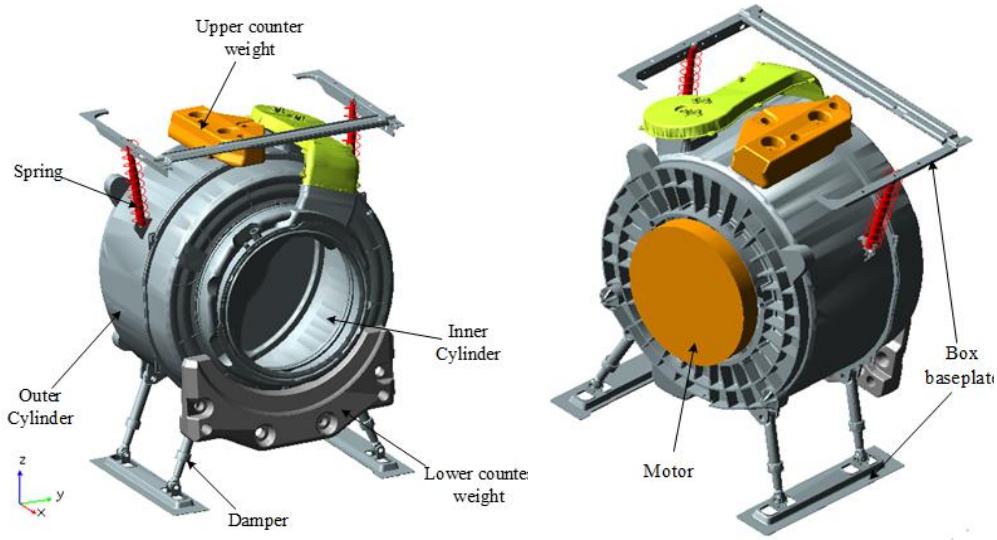

Figure 2. Virtual prototype simulation model of suspension system: **(a)** Front of simulation model; **(b)** Back of simulation model.

3.2.2. Vibration amplitude simulation and validation of suspension system

The amplitude of the suspension system is determined using ADAMS by measuring the displacement of the outer cylinder centroid along the Y direction after establishing the virtual prototype numerical model of the suspension system. The Y direction corresponds to the direction in which the suspension system impacts the box, as depicted in **Figure 2a**.

Figure 3 displays the simulation and experimental curves depicting the outer cylinder amplitude of the suspension system over time. The acceleration process of the suspension system in the simulation differs from that in the experiment, although both reach the same stable speed. The stable segment of the amplitude in the simulation curve corresponds to the steady-state speed of the suspension system, while the speed corresponding to the peak amplitude in the experimental curve represents this stable speed. This observation indicates that the amplitude of the simulation curve closely matches that of the experimental curve upon reaching steady speed, thus allowing for judgment of the validity and accuracy of the virtual prototype simulation model of the suspension system.

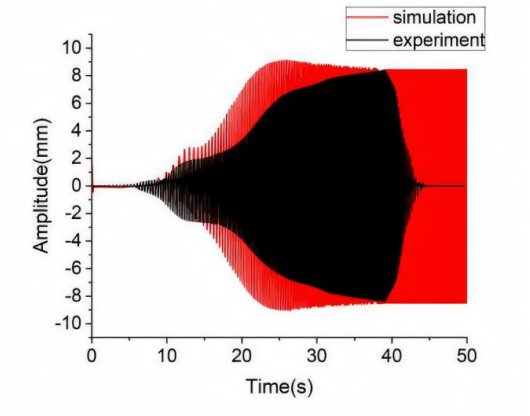

Figure 3. The variation curve of the amplitude with time.

3.3. Prediction analysis of the suspension system amplitude using GA-SVR

3.3.1. Prediction of suspension system amplitude under different structural parameters

27 groups of data were collected for the Taguchi method-based design of experiment used as the sample data for machine learning. Among these, 20 groups were randomly selected as the training set, and the remaining 7 groups were used as the test set. SVR, random forest regression and Backpropagation Neural Network (BP neural network) network models were employed to model and predict based on the 27 groups of data to explore the effectiveness of SVR. Besides, Genetic Algorithm (GA), PSO and Gradient Search (GS) were used to optimize SVR parameters. GA-SVR, PSO-SVR, and GS-SVR models were then used for prediction to demonstrate the effectiveness of GA-SVR.

The performance of modeling and prediction by GA-SVR, PSO-SVR, GS-SVR, random forest regression, and BP neural network is illustrated in **Figures 4–8**. The results are shown in **Tables 3** and **4**. As seen from **Figures 4–8**, compared with PSO-SVR, GS-SVR, random forest regression, and BP neural network, the prediction performance of the GA-SVR model is superior. The prediction performance of different machine learning models is compared and presented in **Figures 9** and **10**. Mean Squared Error (MSE) is used to evaluate the dispersion of prediction results, and R-squared (R^2) is used to evaluate the linear correlation between predicted and measured values. The values of MSE and R^2 indicate better prediction performance. As shown in **Figures 9** and **10**, the prediction performance of SVR is significantly better compared to random forest regression and BP neural network. Furthermore, GA-SVR demonstrates superior performance in modeling and prediction compared to PSO-SVR and GS-SVR, highlighting the effectiveness and accuracy of GA-SVR.

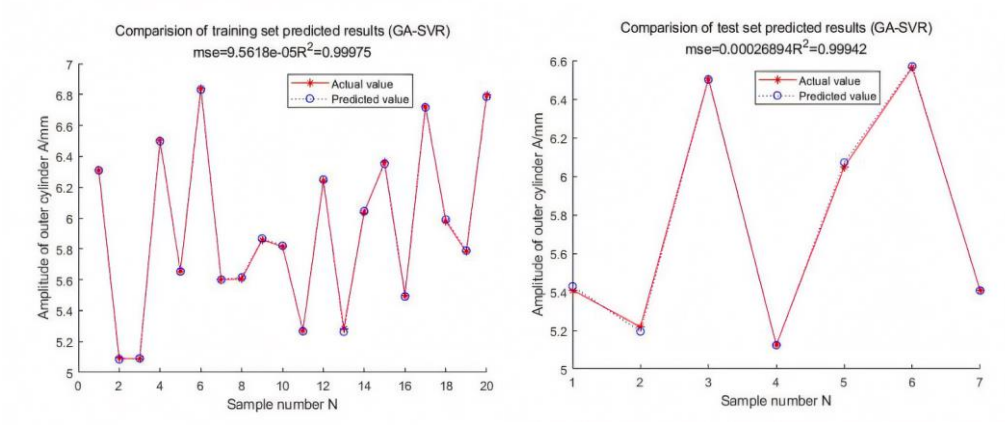

(a) **(b)**

Figure 4. The performance of modeling and predicting using GA-SVR: **(a)** Training set predicted results; **(b)** Test set predicted results.

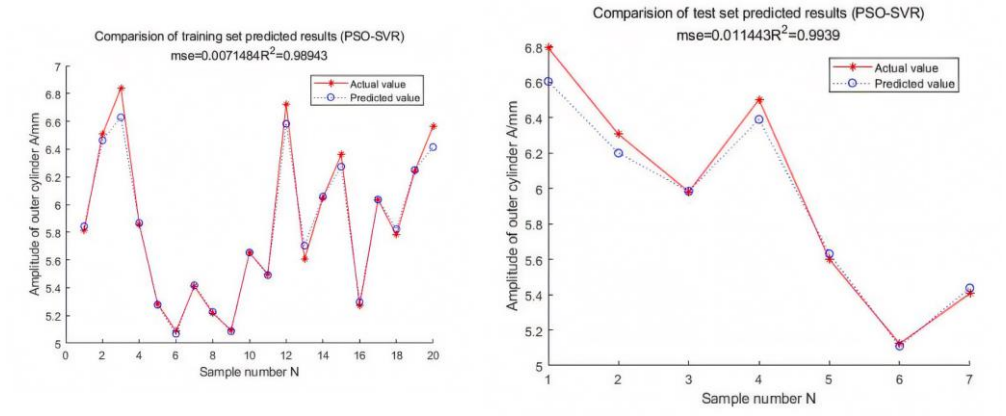

(a) **(b)**

Figure 5. The performance of modeling and predicting using PSO-SVR: **(a)** Training set predicted results; **(b)** Test set predicted results.

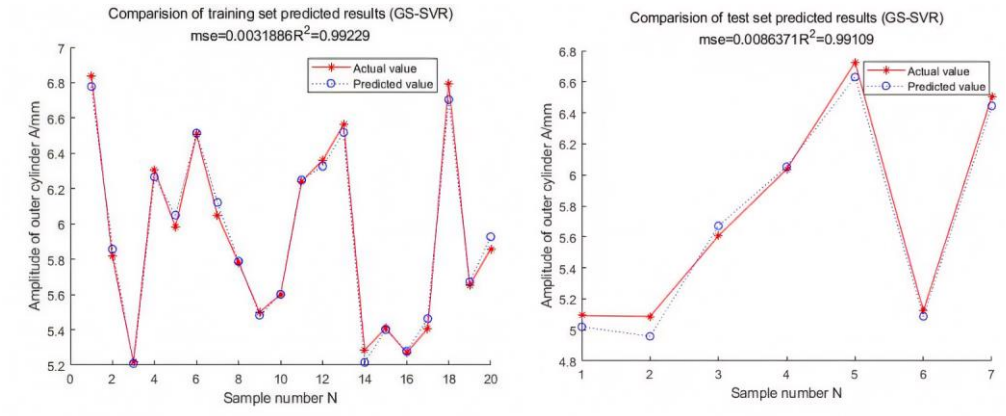

(a) **(b)**

Figure 6. The performance of modeling and predicting using GS-SVR: **(a)** Training set predicted results; **(b)** Test set predicted results.

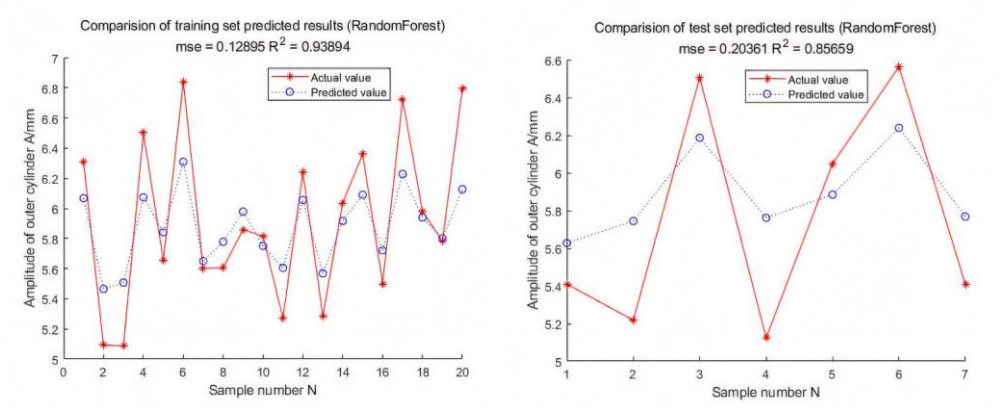

(a) **(b)**

Figure 7. The performance of modeling and predicting using Random Forest Regression: **(a)** Training set predicted results; **(b)** Test set predicted results.

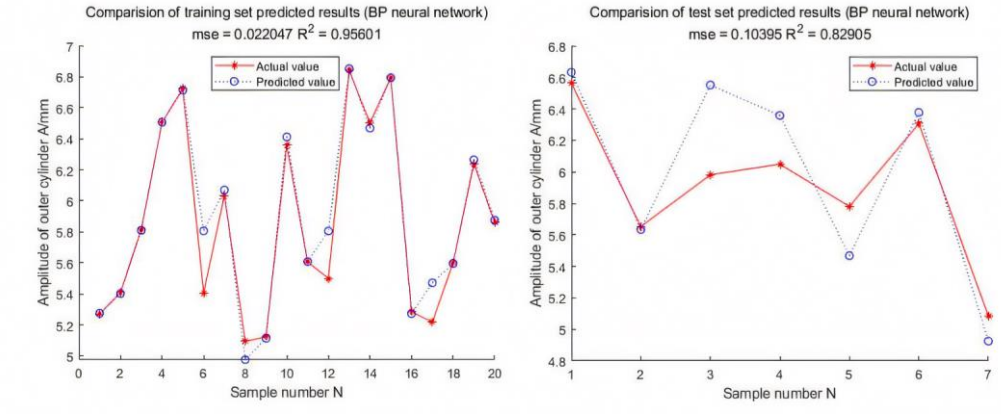

(a) **(b)**

Figure 8. The performance of modeling and predicting using BP neural network: **(a)** Training set predicted results; **(b)** Test set predicted results.

Table 3. Training set prediction results.

Method	**Mean Squared Error (MSE)**	**R-squared (R^2)**
GA-SVR	0.000095618	0.99975
PSO-SVR	0.0071484	0.98943
GS-SVR	0.0031886	0.99229
Random forest regression	0.12895	0.93894
BP neural network	0.022047	0.95601

Table 4. Predictive results of the prediction set.

Method	**Mean Squared Error (MSE)**	**R-squared (R^2)**
GA-SVR	0.00026894	0.99942
PSO-SVR	0.011443	0.9939
GS-SVR	0.0086371	0.99109
Random forest regression	0.20361	0.85659
BP neural network	0.10395	0.82905

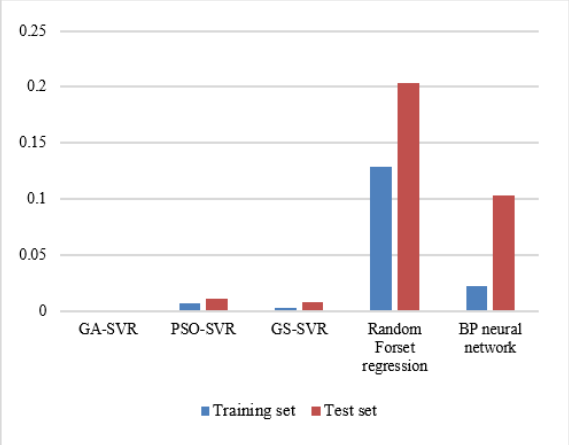

Figure 9. Comparison of MSE prediction results of different machine learning models.

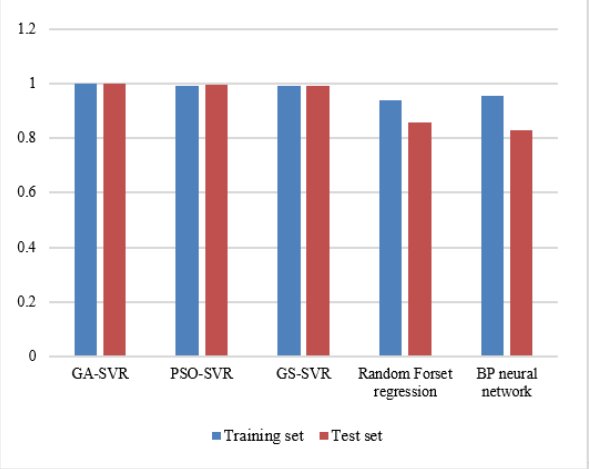

Figure 10. Comparison of R^2 prediction results of different machine learning models.

3.3.2. Prediction of suspension system amplitude under different data sets

Thirty groups of data were collected in the design of experiments based on the response surface method and used as the sample data for machine learning to explore the robustness of GA-SVR. Among these, 22 groups were randomly selected as the training set, and the remaining 8 groups were used as the test set. The corresponding results of modeling and predicting performance are presented in **Figure 11**. The results in **Figure 11** indicate that the MSE and R^2 for the training set predictions are 0.000093766 and 0.99969, respectively, while for the test set predictions, the MSE and R^2 are 0.006162 and 0.99158. As can be seen qualitatively from **Figure 11**, GA-SVR has good predictive performance in both test set and training set. The prediction performance comparison of GA-SVR under different data sets is presented in **Table 5**, which demonstrates the robustness of GA-SVR.

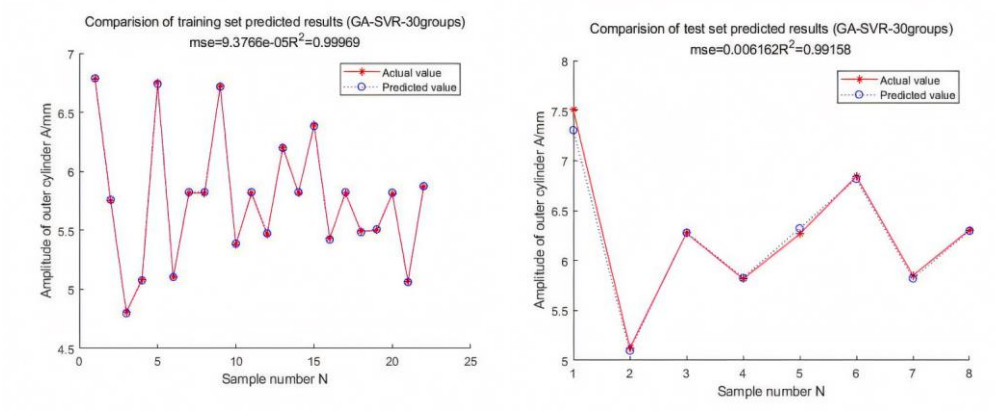

(a) **(b)**

Figure 11. The performance of modeling and predicting using GA-SVR for data set with 30 groups: **(a)** Training set predicted results; **(b)** Test set predicted results.

Table 5. The prediction performance comparison of GA-SVR under different data sets.

		The data set based on Taguchi experimental design-27 groups	**The data set based on response surface experimental design-30 groups**
Training set	MSE	0.000095618	0.000093766
	R^2	0.99975	0.99969
Test set	MSE	0.00026894	0.006162
	R^2	0.99942	0.99158

3.3.3. Prediction of the suspension system amplitude under different operating conditions

Prediction research on suspension system amplitude was conducted under various operating conditions. The operating conditions and factor levels of the washing machine are presented in **Table 6**, and a sample of 25 groups of data was obtained using the Taguchi method-based design of experiments. Among these, 18 groups were randomly selected as the training set, and the remaining 7 groups were designated as the test set. GA-SVR was employed to model and predict using the 25 groups of data. The corresponding results of modeling and prediction performance are presented in **Figure 12**. The results in **Figure 12** indicate that the MSE and R^2 for the training set predictions are 0.0023113 and 0.99541, respectively, while for the test set predictions, the MSE and R^2 are 0.0017751 and 0.9954. These results underscore the effectiveness and accuracy of GA-SVR under different operating conditions.

Table 6. Washing machine operating conditions and factor levels.

Factor levels	**Dehydration speed n/(r/min)**	**Eccentric mass m_0/(kg)**
1	400	0.5
2	500	0.8
3	600	1
4	700	1.2
5	800	1.5

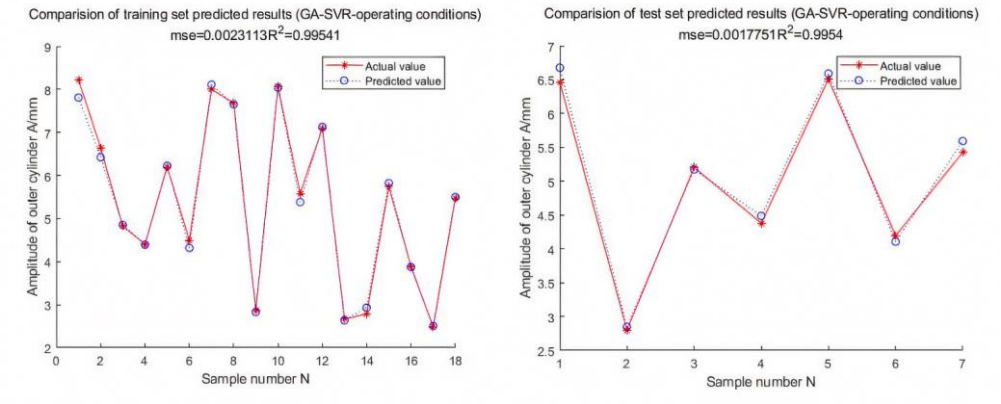

(a) **(b)**

Figure 12. The performance of modeling and predicting using GA-SVR under different operating conditions: **(a)** Training set predicted results; **(b)** Test set predicted results.

3.4. Optimization of the suspension system structural parameters using MOPSO-entropy weight-TOPSIS

The MOPSO-entropy weight-TOPSIS method was employed to solve the multi-objective optimization model, selecting a group of solutions with the best comprehensive performance from the Pareto solution sets as the optimal design scheme for the suspension system. Besides, the NSGA-II-entropy weight-TOPSIS and MOEA/D-entropy weight-TOPSIS were used to solve the multi-objective optimization model and identify the best structural parameters for illustrating the effectiveness of MOPSO-entropy weight-TOPSIS. The parameters settings of the multi-objective optimization algorithm of MOPSO, Non-dominated Sorting Genetic Algorithm II (NSGA-II) [21] and Multi-Objective Evolutionary Algorithm based on Decomposition (MOEA/D) [22] are presented in **Table 7**.

Table 7. Parameters setting of the multi-objective optimization algorithm.

	MOPSO	**NSGA-II**	**MOEA/D**
Population size	100	100	100
Maximum iterations	100	100	100
Neighbor size	/	/	20
Archive size	100	/	/
Mutation probability	/	0.1	/
Crossover probability	/	0.9	/
Inertia factor	0.5	/	/

The Pareto frontier distribution solved by above multi-objective optimization algorithms is presented in **Figure 13**. The performance of above multi-objective algorithms was quantitatively evaluated using two metrics: the Spread of Non-dominated Solution (C_{SNS}) and Mean Ideal Distance (C_{MID}) [23]. The C_{SNS} characterizes the dispersion of the Pareto frontier, where a larger value means a more decentralization of the non-dominated solution set, and better performance of the corresponding multi-objective optimization algorithm. The C_{MID} measures the distance

between the Pareto solution set and the ideal best solution (0,0), where the smaller the value means the shorter distance between the non-dominated solution and the ideal best solution (0,0), and the better performance of the corresponding multi-objective optimization algorithm. The quantitative comparison of these performance indicators of three multi-objective optimization algorithms is presented in **Table 8**. The total mass of the counter weight M and the amplitude of the outer cylinder A were normalized before calculating the performance indicators to eliminate the influence of dimensionality on the comparison results. The values for spread of non-dominated solutions and mean ideal distance are as follows:

$$C_{SNS} = \sqrt{\frac{1}{N-1}\sum_{i=1}^{N}(C_{MID} - \sqrt{f_{1i}^2 + f_{2i}^2})^2} \tag{20}$$

$$C_{MID} = \frac{1}{N}\sum_{i=1}^{N}\sqrt{f_{1i}^2 + f_{2i}^2} \tag{21}$$

where N is the number of non-dominated solutions in the Pareto frontier, f_{1i} and f_{2i} are the fitness of ith solution in the Pareto frontier, respectively.

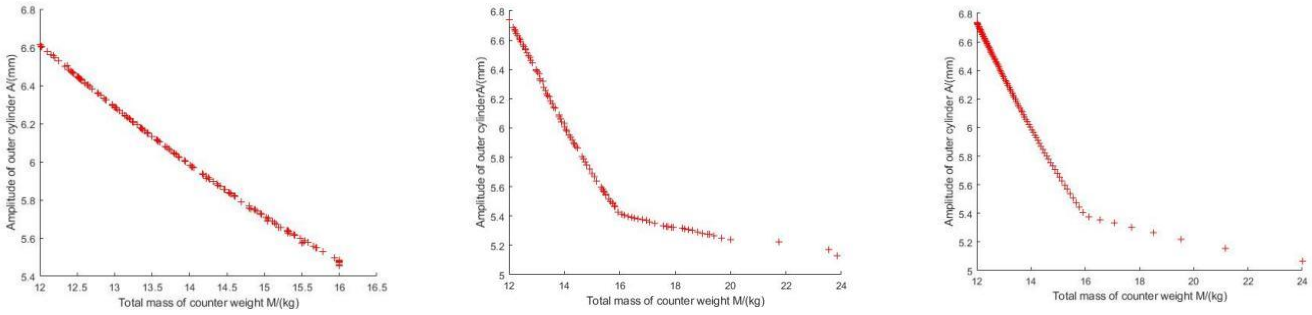

(a) **(b)** **(c)**

Figure 13. Pareto frontier distribution: **(a)** MOPSO; **(b)** NSGA-II; **(c)** MOEA/D.

Table 8. Quantitative comparison of multi-objective optimization algorithm performance.

	Multi-objective optimization algorithm		
	MOPSO	NSGA-II	MOEA/D
C_{MID}	0.8122	0.8389	0.9563
C_{SNS}	0.4184	0.2461	0.2751

As shown in **Table 6**, in term of C_{MID} comparison results, the value of MOPSO is the minimum among the aforementioned algorithms, indicating the shortest distance between the non-dominated solutions of MOPSO and the ideal best solution (0,0). In term of C_{SNS} comparison results, the value of MOPSO is the maximum among the aforementioned algorithms, implying that the Pareto frontier distribution of MOPSO is the best. Meanwhile, it can be found from **Figure 13** that MOPSO has the best distribution uniformity of Pareto boundary. Therefore, MOPSO has the best

comprehensive performance in solving the suspension system multi-objective optimization model among the above the three algorithms mentioned above.

The entropy weight-TOPSIS method was utilized to make multi-objective decisions on the Pareto frontier obtained by the three aforementioned multi-objective optimization algorithms. **Table 9** presents the entropy values and weight coefficients of performance indices calculated using the entropy weight method. The partial solutions of MOPSO, NSGA-II, and MOEA/D, along with their ranking results calculated by entropy weight-TOPSIS, are detailed in **Tables 10** to **12**, respectively, where M is the total weight, M_1 is the upper weight, and M_2 is the lower weight. In these tables, a ranking of 1 indicates the optimal suspension system structural parameters, total mass of counterweight, and amplitude obtained through the calculations. For ease of comparison, the results of the optimization schemes obtained by the three methods above were compared with the empirical design scheme, as shown in **Table 13**.

Table 9. Entropy value and weight coefficient of suspension system performance indexes.

Performance indexes	NSGA-II-entropy weight-TOPSIS		MOPSO-entropy weight-TOPSIS		MOEA/D-entropy weight-TOPSIS	
	Entropy	Weight coefficient	Entropy	Weight coefficient	Entropy	Weight coefficient
Total mass of counter weight M(kg)	0.9915	0.2448	0.9896	0.2157	0.9962	0.0918
Amplitude of outer cylinder A(mm)	0.9739	0.7552	0.9622	0.7843	0.9621	0.9082

Table 10. Partial solutions of MOPSO and sorting results calculated by entropy weight-TOPSIS.

K/(N/mm), C(N·s/mm), M_1/kg, M_2/kg	M/kg, A/mm	Rank
8, 0.2, 5.7244, 8	13.7244, 6.0655	24
8.0073, 0.2667, 5.1996, 8	13.1996, 6.2273	38
8, 0.2010, 5.2424, 8	13.2424, 6.2109	36
8.0108, 0.2012, 4.5434, 8	12.5434, 6.4331	62
8.0002, 0.2169, 4.1763, 8	12.1763, 6.5587	83
8.0013, 0.2578, 8, 8	16, 5.4551	1
8, 0.2055, 5.2483, 8	13.2483, 6.2095	35
8.0002, 0.2019, 7.3031, 8	15.3031, 5.6404	4

Table 11. Partial solutions of NSGA-II and sorting results calculated by entropy weight-TOPSIS.

K/(N/mm), C(N·s/mm), M_1/kg, M_2/kg	M/kg, A/mm	Rank
8.1245, 0.3983, 8, 10.7545	18.7545, 5.2485	9
8.2786, 0.4, 8, 9.5639	17.5639, 5.3043	8
9.4257, 0.4, 6.5196, 8.0477	14.5673, 5.8418	57
8.6129, 0.2061, 4.5072, 8	12.5072, 6.5438	89
8.1265, 0.3989, 8, 10.4053	18.4053, 5.2640	1
9.4586, 0.4, 6.0734, 8.0109	14.0844, 5.9957	64
9.5737, 0.3989, 7.6286, 8.0012	15.6298, 5.5038	40
8, 0.4, 7.9928, 8	15.9928, 5.3802	29

Table 12. Partial solutions of MOEA/D and sorting results calculated by entropy weight-TOPSIS.

K/(N/mm), C(N·s/mm), M_1/kg, M_2/kg	M/kg, A/mm	Rank
8, 0.4, 8, 16	24, 5.0577	1
8, 0.4, 8, 13.1073	21.1073, 5.1508	2
8.0932, 0.3990, 8, 11.5737	19.5737, 5.2126	3
8, 0.4, 8, 10.49	18.49, 5.2583	4
8, 0.4, 8, 9.6701	17.6701, 5.2961	5
8.1992, 0.4, 8, 9.0951	17.0951, 5.3259	6
8.2468, 0.4, 8, 8.5695	16.5695, 5.3524	7
8, 0.4, 8, 8.1224	16.1224, 5.3721	8

Table 13. Comparison between optimization schemes and empirical design scheme.

	K/(N/mm)	C(N·s/mm)	M_1/kg	M_2/kg	M/kg	A/mm
NSGA-II-entropy weight-TOPSIS	8.1265	0.3989	8	10.4053	18.4053	5.2640
MOPSO-entropy weight-TOPSIS	8.0013	0.2578	8	8	16	5.4551
MOEA/D-entropy weight-TOPSIS	8	0.4	8	16	24	5.0577
empirical design scheme	10.5	0.2	5.1251	12.1436	17.2687	6.2469

As shown in **Table 13**, compared to the empirical design scheme which consists of design parameters initially determined by engineers based on existing design standards and specifications, the optimal scheme obtained by NSGA-II-entropy weight-TOPSIS results in a 6.58% increase in the total mass of the counterweight and a 15.73% decrease in the amplitude of the outer cylinder. Similarly, compared to the empirical design scheme, the optimal scheme obtained by MOPSO-entropy weight-TOPSIS shows a 7.35% decrease in the total mass of the counterweight and a 12.68% decrease in the amplitude of the outer cylinder. In contrast, compared to the empirical design scheme, the optimal scheme obtained by MOEA/D-entropy weight-TOPSIS exhibits a 38.98% increase in the total mass of the counterweight and a 19.04% decrease in the amplitude of the outer cylinder. Based on the above analysis, the optimal scheme obtained by MOPSO-entropy weight-TOPSIS achieves a simultaneous reduction in both the amplitude of the outer cylinder and the mass of the counterweight among the three optimal schemes, highlighting the effectiveness of the MOPSO-entropy weight-TOPSIS method.

Based on the analysis of the simulation results, it can be concluded that the stable amplitude of the simulation results is basically consistent with the experimental results, which reflects the rationality and accuracy of the simulation results. Therefore, the errors were calculated between the optimization results obtained by the three methods mentioned above and the simulation results for comparison. The comparison results are shown in **Table 14**, and the average error of the comparison results is 0.33%, which illustrates the rationality of the optimization results.

Table 14. Comparison between optimization and simulation results.

	Structural parameters				Optimization results	Simulation results	Error (%)
	K/(N/mm)	C(N·s/mm)	M_1/kg	M_2/kg	A/mm	A'/mm	
NSGA-II-entropy weight-TOPSIS	8.1265	0.3989	8	10.4053	5.2640	5.2812	0.3
MOPSO-entropy weight-TOPSIS	8.0013	0.2578	8	8	5.4551	5.4331	0.4
MOEA/D-entropy weight-TOPSIS	8	0.4	8	16	5.0577	5.0713	0.3

4. Conclusion and future work

This paper addresses the inherent limitations of traditional methods in optimizing vibration amplitude reduction, such as low calculation accuracy and computational inefficiency, by proposing an innovative approach that synergistically integrates virtual prototyping with machine learning. The effectiveness of this method is validated through a detailed case study on the suspension system of a washing machine, with the following key achievements and results clearly summarized and supported by empirical data:

(1) Introduction of a novel optimization methodology for vibration amplitude reduction that seamlessly combines data-driven techniques with rigorous numerical simulations. By integrating high-fidelity numerical models with state-of-the-art machine learning algorithms, this approach substantially enhances both the accuracy and computational efficiency, overcoming the limitations of traditional optimization methods and providing a more scalable solution.

(2) Development, validation, and application of a robust vibration amplitude prediction model using SVR, specifically tailored for scenarios where sample data is sparse or limited. Through comprehensive analysis of diverse datasets under varying operational conditions, and rigorous comparative assessments with other machine learning techniques, the study conclusively demonstrates the superior predictive accuracy and robustness of SVR in optimizing vibration amplitudes, particularly in real-world engineering applications.

The application of this methodology to the washing machine suspension system resulted in substantial improvements: a 12.68% reduction in vibration amplitude and a 7.35% decrease in the total weight of the counterweight compared to the original design scheme. These results underscore the method's effectiveness in achieving intelligent and efficient design optimization for vibration amplitude reduction, thereby enhancing the suspension system's stability and contributing to more durable and cost-effective washing machine designs. By reducing vibration amplitude and the required counterweight, the methodology not only improves user experience through greater operational stability but also enables a lightweight design that supports extended product life, lower manufacturing costs, and overall energy efficiency.

The design optimization method for vibration amplitude reduction proposed in this paper primarily targets small offline data sets. In the future, combining real-time data acquisition with deep learning algorithms will be further explored. This would make the optimization process even more adaptive to real-time conditions, potentially leading to a more dynamic design process for washing machine suspension systems and other similar applications. A more efficient and adaptive approach to vibration

amplitude reduction will offer substantial improvements in product performance and sustainability.

Author contributions: Conceptualization, HB and JY; methodology, JY; software, JT; validation, HB, JT and JY; formal analysis, JY; investigation, BC; resources, LZ; data curation, JT; writing—original draft preparation, JY; writing—review and editing, JT; visualization, JT; supervision, HB; project administration, HB; funding acquisition, LZ. All authors have read and agreed to the published version of the manuscript.

Funding: This research is supported by the financial support of the National Natural Science Foundation of China (Grant No. 12474462); the Anhui Provincial Natural Science Foundation (Grant No. 2308085ME162); National Natural Science Foundation of China (51505119).

Conflict of interest: The authors declare no conflict of interest.

References

1. Wang, H., Liu L. (2017). Dynamics Modeling and Experiments of Horizontal-axis Washing Machine Suspension System. China Mechanical Engineering, 28(11), 1305-1311.
2. Kim, Y. J., Kim, D. C., Jeong, W. B. (2019). Dynamic modeling and analysis of a quad horizontal damper system for transient vibration reduction in top loading washing machine. Journal of Mechanical Science and Technology, 33, 1123-1130.
3. Mendoza-Flores, S., Velázquez-Villegas, F., Cuenca-Jiménez, F. (2024). Optimization of a Horizontal Washing Machine Suspension System: Studying a 7 DOF Dynamic Model Using a Genetic Algorithm Through a Bounding Box Fitness Function. Journal of Vibration Engineering & Technologies, 12(4), 6865-6884.
4. Tong, Z., Wu, W., Guo, B., Zhang, J., He, Y. (2023). Research on vibration damping model of flat-head tower crane system based on particle damping vibration absorber. Journal of the Brazilian Society of Mechanical Sciences and Engineering, 45(10), 557.
5. Cha, S. T., Baek W. K. (2014). Optimum Suspension System Design for a Drum-typed Washing Machine. Journal of Power System Engineering, 18(3), 20-28.
6. Xiao, L., Zhang, S. (2017). Analysis and optimization of drum washing machine vibration isolation system based on rigid-flexible virtual prototype model. Journal of Vibroengineering, 19(3), 1653-1664.
7. Le, T. D., Nguyen P. T. (2017). Dynamic simulation of seat suspension system with virtual prototyping technology. Journal of Advanced Mechanical Design Systems and Manufacturing, 11(5), 17-00320.
8. Totu, V., Alexandru, C. (2021). Multi-criteria optimization of an innovative suspension system for race cars. Applied Sciences, 11(9), 4167.
9. Wang, H., Chang, L., Tian, Y. (2021). Extended state observer–based backstepping fast terminal sliding mode control for active suspension vibration. Journal of Vibration and Control, 27(19-20), 2303-2318.
10. Guan, D., Wu, J., Li, J., Yang, Z., Yurchenko, D. (2024). Parameter Analysis of Vibration Damping and Energy Harvesting Performance of Bionic Suspension. International Journal of Applied Mechanics, 16(4), 2450048.
11. Kashfi, M., Goodarzi S., Rastgou M. (2022). Plastic properties determination using virtual dynamic spherical indentation test and machine learning algorithms. Journal of Mechanical Science and Technology, 36(1), 325-331.
12. Yu, K. H., Shiu S. C., Liu C. W. (2022). Development of surrogate models of clamp configuration for optical glass lens centering through finite element analysis and machine learning. International of Advanced Manufacturing Technology, 121(11-12), 8209-8220.
13. Noh, E., Hong S. (2022). Finite element analysis and support vector regression-based optimal design to minimize deformation of indoor bicycle handle frame equipped with monitor. Applied Science, 12 (6), 2999.
14. Huri, D., Mankovits T. (2020). Parameter selection of local search algorithm for design optimization of automotive rubber bumper. Applied Science, 10(10), 3584.

15. Liu, B. E., Yu W. (2020). On-demand direct design of polymeric thermal actuator by machine learning algorithm. Chinese Journal of Polymer Science, 38(8), 908-914.
16. Smola, A. J., Schölkopf, B. (2004). A tutorial on support vector regression. Statistics and computing, 14, 199-222.
17. Chang, C. C., Lin C. J. (2011). LIBSVM: a library for support vector machines. ACM Transactions on Intelligent Systems and Technology, 2(3),1-27.
18. Coello, C. A. C., Pulido, G. T. Lechuga M. S. (2004). Handing Multiple Objectives With Particle Swarm Optimization. IEEE Transactions on Evolutionary Computation, 8(3), 256-279.
19. Chen, J. Q. (2019). Fault prediction of a transformer bushing based on entropy weight TOPSIS and gray theory. Computing in Science & Engineering, 21(6), 55-62.
20. Huang, J. (2008, September). Combining entropy weight and TOPSIS method for information system selection. In 2008 ieee conference on cybernetics and intelligent systems (pp. 1281-1284). IEEE.
21. Yusoff, Y., Ngadiman M. S., Zain A. M. (2011). Overview of NSGA-II for optimizing machining process parameters. Procedia Engineering, 15, 3978-3983.
22. Qi, Y. T., Ma X. L., Liu F., Jiao L. C., Sun J. Y., Wu J. S. (2014). MOEA/D with adaptive weight adjustment. Evolutionary Computation ,22(2), 231-264.
23. Behnamian, J., Zandieh M., Ghomi S. M. T. F. (2010). A multi-phase covering pareto-optimal front method to multi-objective parallel machine scheduling. International Journal of Production Research, 48(17), 4949-4976.